

# Multiscale Mechanics of Graphene Fracture

Comparing Empirical and Machine Learning Potentials,  
Benchmarked with Quantized Fracture Mechanics

Hanfeng Zhai

Cornell University

September 16, 2022



Project #2 for Master Thesis

# Content

- **Background**

What is the problem? Why do we care? What is the core novelty?  
Potential applications & impacts.

- **Methodology**

Empirical potentials (REBO, AIREBO, AIREBO-M, optimized Tersoff); ML potentials; QFM.

- **Results & Discussion**

Benchmarking QFM; Anomalous fracture forms; Benchmarking ML potentials; Physico-Chemical Mechanics.

- **Main Takeaways**

Major findings & conclusions. Some interesting thoughts.

- **Future Outlook**

How this work may potentially lead to my Ph.D. research.

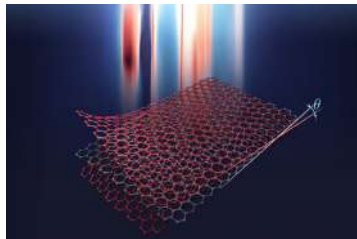
# Background

## *What is the problem?*

### Graphene: A Wonder Material

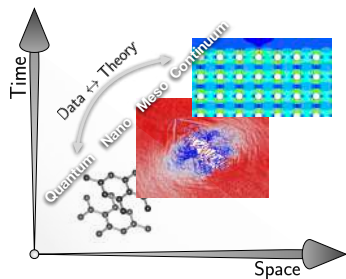
#### Superior Properties

- High Toughness
- High Thermal Conductivity
- Good Electrical Conductivity
- Abundant Studies & Nobel Prize
- Multiple Theories Based Upon



Credit: Siliezar, *The Harvard Gazette*, 2021

### Multiscale Computational Modeling



#### Multiscale Theories

- Density Functional Theory (*ab initio*)
- Molecular Dynamics
- CG, DPD, DEM, ... (Mesoscale)
- (Sub-) Continuum Mechanics

# Background

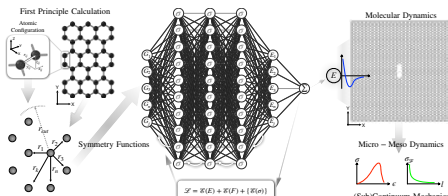
*...some theoretical backgrounds*

## Quantum Mechanics → DFT

Governing equation for quantum mechanics,  
i.e. Schrödinger equation:

$$\mathbf{H}|\Psi\rangle = \mathbf{E}|\Psi\rangle$$

DFT simplifies the S.E. based on 3 approxos.

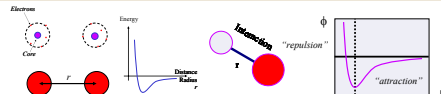


## Molecular Dynamics

Molecular interaction potentials based on  
the idea of “attraction + repulsion”:

$$\mathbf{E} = f_{\text{cut}}(\mathbf{E}_R + \mathbf{E}_A)$$

where the cutoff  $f_{\text{cut}}$  play essential role in  
fracture of non-bonded potentials.



Credit: Buehler, MIT DSpace, 2006

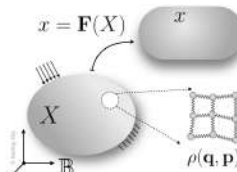
## Continuum Mechanics

Assume a deformation mapping in a 3D space:  $\mathbf{x} \rightarrow \mathbf{X}$ ; one can compute displacement  $\mathbf{u} = \mathbf{x} - \mathbf{X}$ , further elicit defor. grad. tensor:

$$\mathbf{F} = \frac{\partial \mathbf{x}}{\partial \mathbf{X}}$$

where the constitutive relation states:

$$\boldsymbol{\sigma} = \Psi(\boldsymbol{\epsilon})$$



# Methodology

## Machine learning potentials



J. Behler



M. Parrinello

Credits: OpenKIM and ETHZ

Proposed fitting molecular potentials using neural networks as universal approximations

PRL 98, 146401 (2007)

PHYSICAL REVIEW LETTERS

week ending  
6 APRIL 2007

### Generalized Neural-Network Representation of High-Dimensional Potential-Energy Surfaces

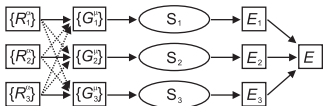
Jörg Behler and Michele Parrinello

Department of Chemistry and Applied Biosciences, ETH Zurich, USI-Campus, Via Giuseppe Buffi 13, CH-8900 Lugano, Switzerland  
(Received 27 September 2006; published 2 April 2007)

The accurate description of chemical systems often requires the use of computationally demanding methods like density-functional theory (DFT), making long simulation of large systems unfeasible. In this Letter we introduce a new kind of neural-network representation of DFT potential-energy surfaces, which provides the energy and forces as a function of all atomic positions in systems of arbitrary size and is several orders of magnitude faster than DFT. The high accuracy of the method is demonstrated for bulk silicon and compared with empirical potentials and DFT. The method is general and can be applied to all types of periodic and nonperiodic systems.

DOI: 10.1103/PhysRevLett.98.146401

PACS numbers: 71.15.Pd, 61.50.Ah, 82.20.Kh



## Theory

The atomic configurations in first principles, i.e., DFT, AIMD, include locations, radius, etc., are transformed into symmetry functions:

$$G_i^R = \sum_{j \neq i}^{\text{all}} \mathcal{F}_R(r_{ij}) f_C(r_{ij}),$$
$$G_i^A = \sum_{j, k \neq i}^{\text{all}} \mathcal{F}_A(r_{ij}, r_{ik}, r_{jk}) f_C(r_{ij}) f_C(r_{ik}) f_C(r_{jk})$$

The output energies are approximated via a neural network of  $L$  layers. The eventually learned energy:  $E = \sum_i E_i$ , where

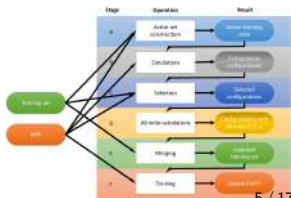
$$E_i = (K_L \circ \sigma_L \circ \dots \circ K_1 \circ \sigma_1 \circ K_0) [G_i^R, G_i^A]$$

Four different such models are adopted to benchmark the molecular simulations.



A. Shapeev

Credit: Shapeev.com



# Methodology

## Potential models

### REBO potential

The reactive bond order (REBO) potential is first proposed by Brenner, is an exclusively short-ranged potential. The interaction is computed only when their distance is less than a covalent-bonding cutoff:

$$E_{ij}^{REBO} = \sum_{j \neq i} f_c^{REBO}(r_{ij}) [V_R(r_{ij}) + \bar{b}_{ij} V_{ij}^A]$$

where  $V_{ij}^R$  and  $V_{ij}^A$  are the repulsive and attractive pairwise potentials between atoms  $i$  and  $j$  determined by  $r_{ij}$ .  $\bar{b}_{ij}$  is the many-body term. The repulsive  $V^R$  and attractive  $V^A$  terms obey:

$$V_{ij}^R = \sum_{n=1}^3 B_n e^{\beta_n r}, \quad V_{ij}^A = \left(1 + \frac{Q}{r}\right) A e^{\alpha r}$$

where  $A$ ,  $B_n$ ,  $\beta_n$ ,  $\alpha$ , ..., are parameters.

### AIREBO potential

Stuart et al. further proposed the adaptive intermolecular REBO (AIREBO) method, adding Leonard-Jones (LJ) and torsional interactions to the total potential:

$$E^{AIREBO} = \frac{1}{2} \sum_i \sum_{j \neq i} \left[ E_{ij}^{REBO} + E_{ij}^{LJ} + \sum_{k \neq i, j} \sum_{l \neq i, j, k} E_{ijkl}^{TOR} \right]$$

### AIREBO-M potential

Further, O'Connor, Andzelm, and Robbins replaced the LJ interactions with the Morse potential to more accurately describe the intermolecular interactions:

$$V_{ij}^{MORSE}(r) = -\epsilon_{ij} \left[ 1 - \left( 1 - e^{\alpha_{ij}(r - r_{ij}^{eq})} \right)^2 \right]$$

The final form of the total energy of AIREBO-M potential is:

$$E^{AIREBO-M} = E^{REBO} + E^{MORSE} + E^{TORS}$$

### Optimized Tersoff potential

In the Tersoff proposition, the potential was fitted to guarantee the universal behavior of calculated energy curves can be mapped to a single dimensionless curve through parameterized rescaling, as shown by Ferrante, Smith, and Rose. Such an interatomic potential is taken the form:

$$E^{TERSOFF} = \sum_i E_i^{TERSOFF} = \frac{1}{2} \sum_{i \neq j} V_{ij}^{TERSOFF},$$

$$V_{ij}^{TERSOFF} = f_C^{TERSOFF}(r_{ij}) [A e^{(-\lambda_1 r_{ij})} - B_{ij} e^{(-\lambda_2 r_{ij})}]$$

# Methodology

## Quantized fracture mechanics

### Theoretical Derivation

Suppose the smallest crack propagation length is  $L_0$ , which for graphene along the zigzag direction should be  $L_0 = 0.246\text{nm}$ ; the initial crack (defect region of graphene) has a length of  $\mathfrak{L}_C = 2\rho$ ;  $\rho$  is the tip radius, which in our case  $\rho = 0.265\text{nm}$ . In continuum-based linear elastic fracture mechanics (LEFM), the fracture is defined to occur while the stress intensity equals its critical value,  $K_I^{\text{LEFM}} = K_{IC}$ . In QFM, the crack propagates when

$$K_I^{\text{QFM}} = \sqrt{\frac{1}{L_0} \int_{\mathfrak{L}}^{\mathfrak{L}+L_0} [K_I^{\text{LEFM}}(\mathfrak{L})]^2 d\mathfrak{L}} = K_{IC}$$

Substituting this  $K_{IC}$ , the fracture stress in QFM writes  $\sigma_F(\mathfrak{L}) = \frac{K_{IC}}{\sqrt{\pi(\mathfrak{L}+L_0/2)}}$ . By extending this fracture stress from sharp to blunt cracks, Pugno & Ruoff finds an asymptotic correction for small tip radii and proposed the form:

$$\sigma_F(\mathfrak{L}, \rho) = K_{IC} \sqrt{\frac{1 + \frac{\rho}{2L_0}}{\pi(\mathfrak{L} + \frac{L_0}{2})}}$$

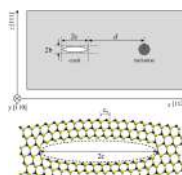


N. Pugno

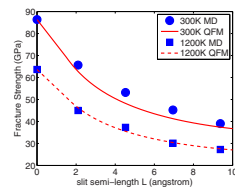


R. Ruoff

Credit: Università di Trento and Wikipedia



Ippolito et al., 2006



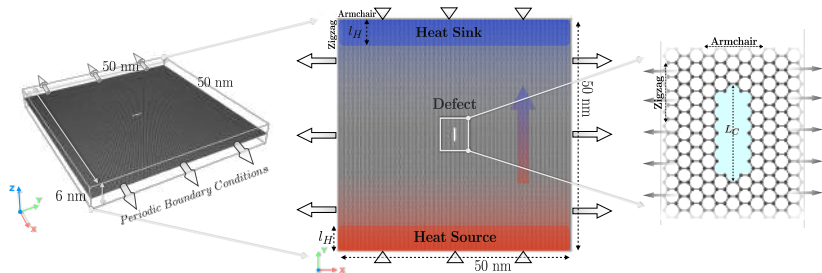
Zhao & Aluru, 2010

### Key Points

- Derived from Griffith's Theory
- Discretized Fracture Process
- Fittable with MD Simulation Data

# Methodology

## Numerical Setup

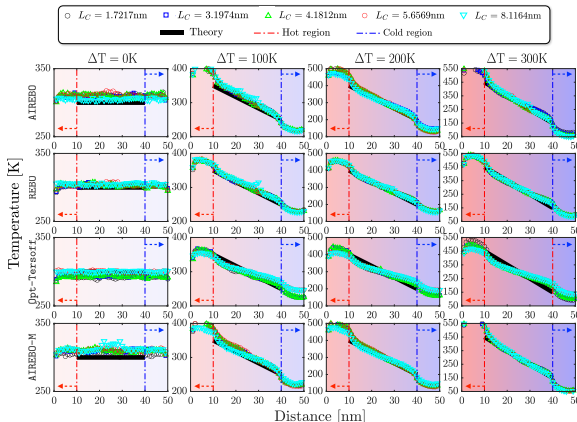


## LAMMPS Implementation

- A three-dimensional simulation box with full PBC of applied strain rate loading implemented in LAMMPS.
- A thermal gradient was applied in the Y direction, including the heat source (bottom) and heat sink (upper side).
- A defect (slit) is set in the center of the graphene layer of different lengths.

# Methods — Verification

## Thermal Gradients: Equilibrium Distribution

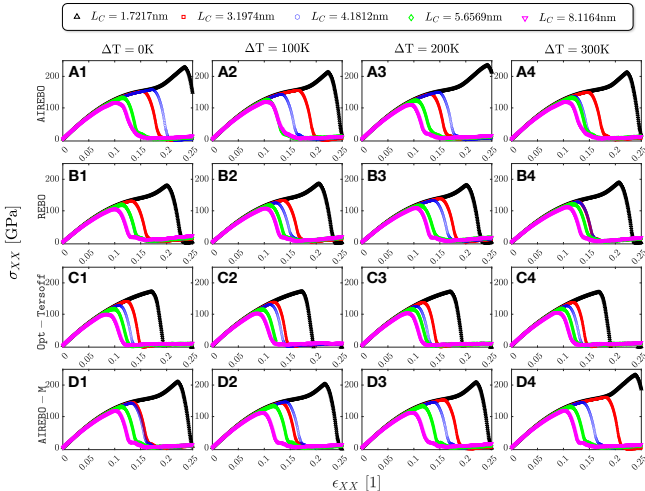


The temperature distribution along with the single graphene layer after 10,000 steps of equilibration run. The scattered dots in different colors represent different graphene layers with different length of preset cracks.

1. Temperature linear distribution.
2. Potential Models' Accuracy
3. Weak Effects of Crack Lengths
4. Effects of Thermal Gradients
5. Coupling Effects...

# Results & Discussion

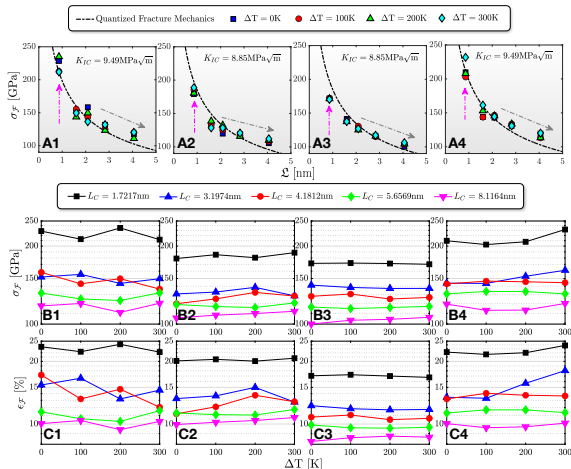
## Mechanical Responses



The stress-strain responses of the graphene sheet during non-equilibrium tensile tests of high strain rate under heat gradients.

# Results & Discussion

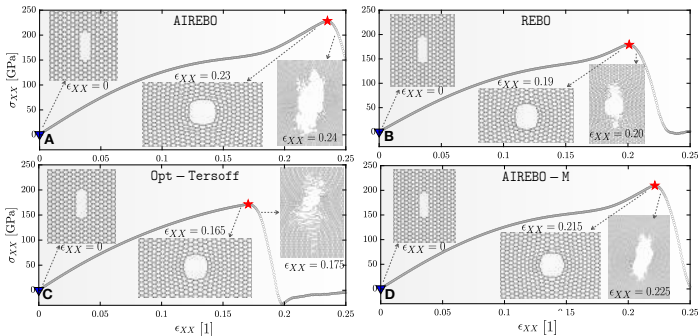
## Quantized Fracture Mechanics



The diagrams of the fracture stresses and strains ( $\sigma_F$  &  $\epsilon_F$ ) of the graphene layer regarding different initial defects lengths and temperature differences.

# Results & Discussion

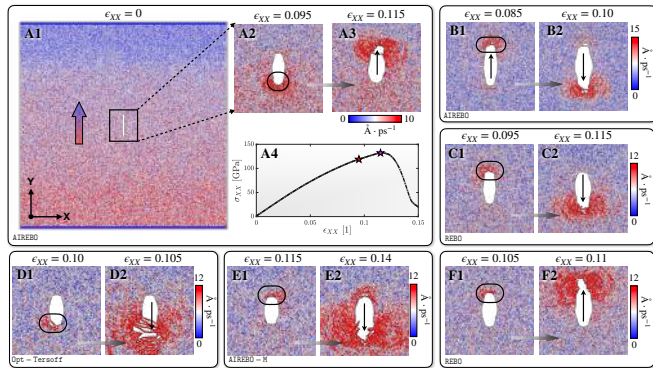
## Physico-Chemical Perspective Nonlinear Mechanics



The stress-strain responses of the graphene sheet using the four different potential fields of a small initial defect ( $L_C = 1.7217\text{nm}$ ). The four subfigures **A**, **B**, **C**, **D** illustrated the deformation and fracture profile along the defected area marked with the corresponding strain values. The red star stands for the fractured moment. The blue triangular dot is the initial morphology of the defect.

# Results & Discussion

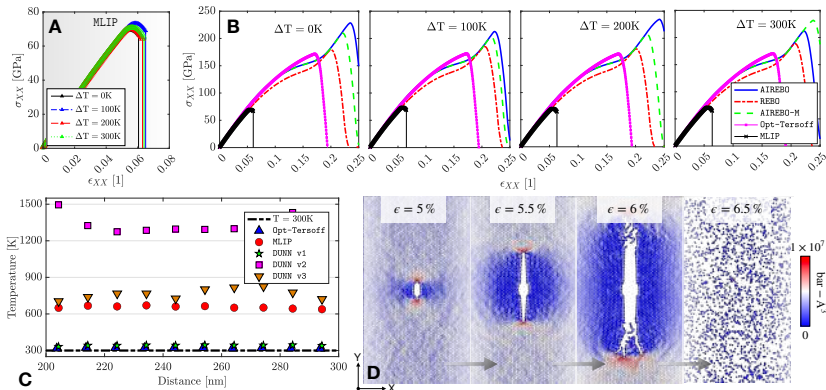
## Abnormal Fracture Characterizations



Graphical illustration of the observed “energy transportation” phenomena during the fracture process. The subfigures **A** to **F** stand for the 6 representative simulation cases to depict the fracture processes. **A1** to **A3** illustrates a typical observed energy transportation process of higher kinetic energy first clustered as one side of crack tip the, and **A4** is a stress-strain response corresponding the process, for which the red and pink stars corresponds to **A2** and **A3**, respectively.

# Results & Discussion

## Benchmarking Machine Learning Potentials



The simulation results for benchmarking the machine learning methods. **A**. The stress-strain responses of the graphene fracture with small defect ( $L_C = 1.7217\text{nm}$ ) using the MLIP potential. **B**. The stress-strain responses comparing the four empirical potentials with MLIP on fracturing the graphene sheet. **C**. The temperature distribution after 10,000 steps of equilibration run with preset 300K constant temperature. **D**. Graphical representation of a typical fracture process based on MLIP potential.

## Main Takeaways

- The stress-strain responses highly depend on potentials. The "REBO-based" potentials exhibit strain-hardening effects for a small defect.
- The fracture direction is reported to be not related to thermal gradients.
- Abnormal fractures are observed for "REBO-based" potentials, where the kinetic energy is transported along the crack tips before fracture.
- The machine learning interatomic potentials show lower fracture stresses.
- The employed trained deep learning potentials lack the ability to describe postfracture molecular dynamical descriptions.

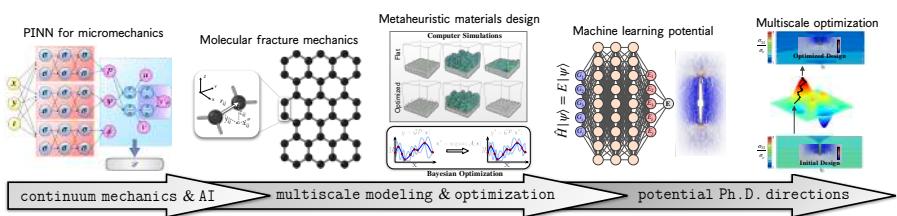
# Future Outlook

## Core Idea of This Work

- Machine Learning Potentials Benchmark and Investigation
- Molecular Dynamics Potential Comparison and Characterization
- Quantized Fracture Mechanics Verification and Benchmark
- Fracture Process Characterization

## Future Work

- Develop Our Own Machine Learning Potentials for Characterizing Dynamics
- Use the Computational Framework to Guide (Heuristic) Materials Design
- “Universal” Data Driven Scale-Bridging for Three Scales



Thank you for listening!

Any Questions?

Hanfeng Zhai

hz253@cornell.edu

[www.hanfengzhai.net](http://www.hanfengzhai.net)